Frequency and Modulation Index Related Effects in Continuous and Discontinuous Modulated Y-Inverter for Motor-Drive Applications

Hamzeh J. Jaber, and Alberto Castellazzi
Kyoto University of Advanced Science
Kyoto, Japan
hamzeh.j.jaber@kuas.ac.jp

Acknowledgments

The authors gratefully acknowledge the support received from Grant 20H02138 of the Japanese Society for the Promotion of Science (JSPS) under the Kakenhi-Kiban-B scheme.

Keywords

≪DC-AC converters ≫, ≪Discontinuous pulse-width modulation≫, ≪GaN transistors≫.

Abstract

The effect of the pulse-width modulation scheme on the efficiency of a three-phase Y-inverter with a wide range of output voltages and currents is investigated experimentally in this paper. The efficiency measurements obtained while conducting experiments on a GaN-based Y-inverter prototype indicate that no pulse-width modulation scheme results in higher efficiency of the Y-inverter over the entire range of motor operation. In other words, depending on the operating conditions, a discontinuous PWM results in a higher or lower efficiency than a continuous sinusoidal PWM. As a result, there is a chance that using a hybrid modulation strategy will improve the efficiency of the Y-inverter. Furthermore, the distortion effect caused by inappropriate inductor and capacitor value selection is highlighted.

Introduction

Higher rotation speed machines with higher pole numbers and smaller size for the same torque ratings will be required to advance the state-of-the-art in electric motor drives. Such requirements translate primarily into the need for higher switching frequency solutions in the electrical power converter, but clearly without sacrificing efficiency. Wide-band-gap (WBG) semiconductors are viewed as key enabling technologies of improvement from this perspective. However, it is now widely accepted that simply replacing silicon (Si) transistors with silicon carbide (SiC) or gallium nitride (GaN) transistors yields incremental benefits but does not fully justify the higher cost of the technology. The following are bottlenecks to fully utilizing WBG semiconductors in conventional power conversion solutions:

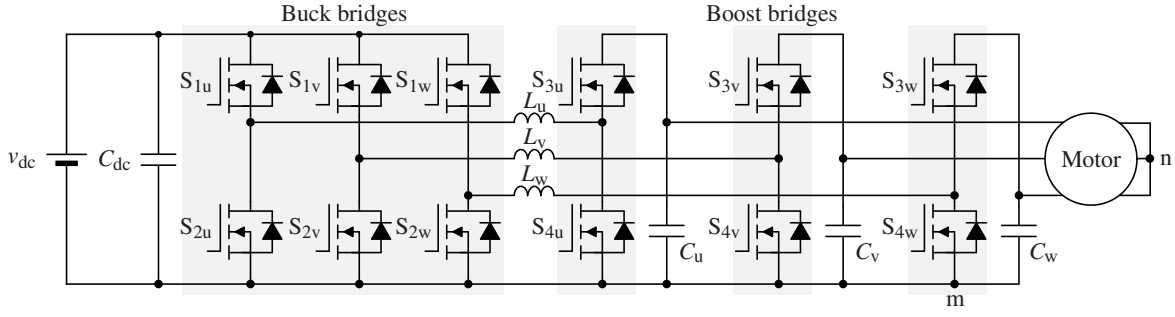

Fig. 1: Circuit configuration of a three-phase buck-boost Y-inverter.

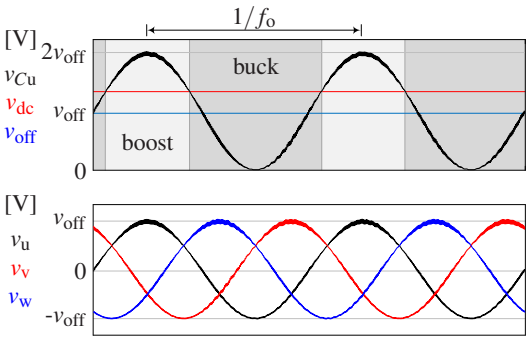

Fig. 2: Illustration of the principle of operation of the Y-inverter.

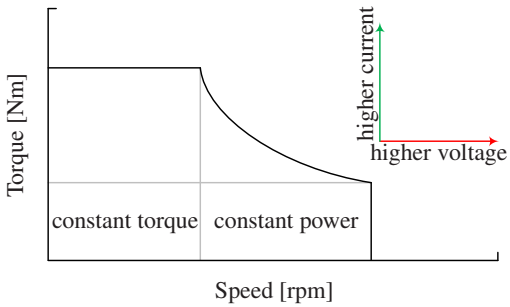

Fig. 3: Torque-speed curve of a permanent magnet synchronous motor.

1. High dv/dt: When going from Si to SiC or GaN, switching transitions can easily be faster by a factor of 10. The much higher dv/dt values pose critical limitations to both functionality (e.g., common mode noise in parasitic capacitance, voltage overshoots, and wave reflections in cables and connectors), and reliability (e.g., degradation of motor winding insulation, and corrosion of motor bearings due to parasitic current flow),
2. Electromagnetic emission: The increase in the switching frequency that can be achieved in established solutions without sacrificing efficiency is closer to a factor of 4 to 5, which means that the spectrum of electromagnetic emission is shifted by the same amount towards higher frequencies. This makes meeting typical emission requirements, which typically impose lower frequency limits, extremely difficult.

To overcome the limitations mentioned above, multilevel inversion has been proposed as an evolutionary solution. Indeed, 3 or 5 level inversion can help to improve voltage inversion performance to some extent. However, the large number of components of the multilevel inverters makes it difficult for such approaches to gain widespread acceptance for use with WBG devices.

Recently, new topologies of two-level inverters have been proposed to exploit the high switching frequency capability of the WBG devices. Specifically, two approaches have been pursued; current source inversion [1, 2] and Y-inversion [3, 4]. The latter is derived from a well-known concept of creating an inverter from 3 Y-connected dc-dc converters, but has recently gained significant momentum, in particular by its implementation as a non-inverting buck-boost converter (4-switch cell). Both topologies do away with the above-mentioned issues, allowing the semiconductor devices to operate at significantly higher switching frequencies. Moreover, both offer built-in voltage boosting capability, so that no boost chopper or dc-link stage are required. They are thus ideal for high-performance motor-drive systems. This paper focuses on the three-phase buck-boost Y-inverter proposed in [3]. In particular, this paper presents an experimental investigation of the impact of the pulse-width modulation (PWM) strategy on the efficiency of a three-phase Y-inverter with a wide range of output voltages and currents.

Three-phase buck-boost Y-inverter

Circuit configuration

Fig. 1 shows the circuit configuration of the three-phase buck-boost Y-inverter (hereinafter referred to as the Y-inverter). Here, v_{dc} represents the dc voltage source, and C_{dc} is the input-side filter capacitor. S_{1u} and S_{2u} are the switching devices of the buck bridge of phase u, S_{1v} and S_{2v} are the switching devices of the buck bridge of phase v, S_{1w} and S_{2w} are the switching devices of the buck bridge of phase w, S_{3u} and S_{4u} are the switching devices of the boost bridge of phase u, S_{3v} and S_{4v} are the switching devices of the boost bridge of phase v, and S_{3w} and S_{4w} are the switching devices of the boost bridge of phase w. L_u, L_v, and L_w are the inductors connected between the middle points of the buck bridges and the boost bridges of phase u, v, and w, respectively. C_u, C_v, and C_w are the output capacitors of phase u, v, and w, respectively. m is the ground, and n is the neutral point of the Y-connected load.

Table I: Experimental circuit parameters used for efficiency measurements.

Parameter	Symbol	Value
Input dc voltage	v_{dc}	140 V
Inductance	L	13.6 µH
Capacitance	C	6 µF
Switching frequency	f_{sw}	100 kHz

Table II: Experimental circuit parameters that corresponds to Fig. 14.

Parameter	Symbol	Value
Input dc voltage	v_{dc}	60 V
Inductance	L	20 µH
Capacitance	C	4.7 µF
Switching frequency	f_{sw}	150 kHz

Principle of operation

The Y-inverter consists of three non-inverting buck-boost converters (NIBB). Each NIBB produces a strictly positive voltage, where the duty ratios of the buck and the boost bridges can be appropriately adjusted to produce a sine-shaped voltage as shown in Fig. 2. Here, v_{Cu} is the voltage across C_u which has a sinusoidal shape with a frequency of f_o, an offset voltage of v_{off}, and a peak-to-peak voltage of $2v_{off}$. The NIBB of phase u operates in the buck mode when $v_{dc} > v_{Cu}$, and in boost mode when $v_{dc} < v_{Cu}$. Similarly, the NIBBs of phase v and phase w generates v_{Cv} and v_{Cw}, respectively, where v_{Cu}, v_{Cv}, and v_{Cw} are $2\pi/3$ radians apart. v_{off} is eliminated from the phase-to-neutral voltages of the Y-connected load.

Experimental investigation of the effect of modulation scheme on efficiency and voltage quality

Fig. 3 shows a typical torque-speed curve of permanent magnet synchronous motor (PMSM). For a wide range of operations, the motor voltages and currents can vary significantly in which a relatively high voltage (corresponds to a relatively low current) and a relatively low voltage (corresponds to a relatively high current) are required for constant-power operation. Therefore, the Y-inverter has to operate under these conditions, where it may be required to produce a peak-to-peak load voltage below or above the dc source voltage.

In [3], sinusoidal PWM (SPWM) and discontinuous PWM (DPWM) schemes were employed for the Y-inverter. It is shown in [3] that the DPWM results in lower switching losses. However, a more careful investigation should be conducted to evaluate the effect of the modulation scheme on the efficiency. For this purpose, experiments were performed on a 3-kW GaN-based Y-inverter prototype to measure the efficiency under various operating conditions.

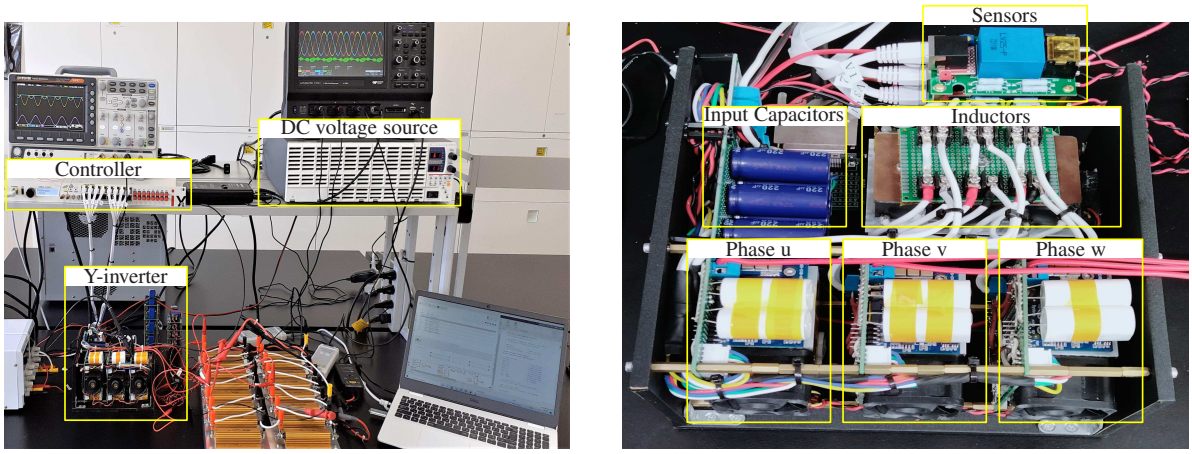

(a) (b)

Fig. 4: Photograph of (a) the experimental setup and (b) the Y-inverter prototype.

Table III: Measured efficiency of the Y-inverter prototype under various operating conditions.

Load RMS voltage	Load voltage frequency	Output power	Modulation scheme	Efficiency
31.8 V	500 Hz	599 W	SPWM	93.97 %
			DPWM	92.54 %
		1184 W	SPWM	97.35 %
			DPWM	94.41 %
49.5 V	1.0 kHz	585 W	SPWM	95.01 %
			DPWM	93.27 %
		1081 W	SPWM	99.11 %
			DPWM	98.73 %
74.2 V	1.5 kHz	601 W	SPWM	87.74 %
			DPWM	90.13 %
		1316 W	SPWM	93.83 %
			DPWM	94.39 %

Experimental conditions

Table I summarizes the experimental circuit parameters used for efficiency measurements, where the experimental setup is shown in Fig. 4 (a), and the Y-inverter prototype is shown in Fig. 4 (b) in which 650-V, 25 mΩ GaN transistors (GS66516B) from GaN Systems are used. Each experiment corresponds to a different set of output capacitor peak voltage, $\hat{v_C}$, frequency, $f_{\rm o}$, load output power, $P_{\rm o}$, and modulation scheme. The following experiments were carried out.

1. $\hat{v_C} = 90\,\text{V}$, $f_{\rm o} = 500\,\text{Hz}$, $P_{\rm o} = 599\,\text{W}$, and both SPWM and DPWM were used.
2. $\hat{v_C} = 90\,\text{V}$, $f_{\rm o} = 500\,\text{Hz}$, $P_{\rm o} = 1184\,\text{W}$, and both SPWM and DPWM were used.
3. $\hat{v_C} = 140\,\text{V}$, $f_{\rm o} = 1.0\,\text{kHz}$, $P_{\rm o} = 585\,\text{W}$, and both SPWM and DPWM were used.
4. $\hat{v_C} = 140\,\text{V}$, $f_{\rm o} = 1.0\,\text{kHz}$, $P_{\rm o} = 1081\,\text{W}$, and both SPWM and DPWM were used.
5. $\hat{v_C} = 210\,\text{V}$, $f_{\rm o} = 1.5\,\text{kHz}$, $P_{\rm o} = 601\,\text{W}$, and both SPWM and DPWM were used.
6. $\hat{v_C} = 210\,\text{V}$, $f_{\rm o} = 1.5\,\text{kHz}$, $P_{\rm o} = 1316\,\text{W}$, and both SPWM and DPWM were used.

In Fig 5 to Fig 12, the waveforms of $d_{\rm u1}$, $d_{\rm u2}$, $v_{C\rm u}$, and $v_{\rm dc}$, are captured by GW Instek MDO-2204EX oscilloscope, and the waveforms of $v_{\rm u}$, $v_{\rm v}$, $v_{\rm w}$, and $i_{L\rm w}$, are captured by WaveSurfer 3104z Teledyne LeCroy oscilloscope. where $d_{\rm u1}$ and $d_{\rm u2}$ are the duty ratios of $\text{S}_{1\rm u}$ and $\text{S}_{3\rm u}$, respectively, and $v_{\rm u}$, $v_{\rm v}$, $v_{\rm w}$, are the phase-to-neutral voltages of phase u, phase v, and phase w, respectively.

Micsig DP10013 voltage probe was used to measure $v_{\rm u}$, Ivytech P5205A voltage probes were used to measure $v_{\rm v}$ and $v_{\rm w}$, Tektronix TRCP0300 current probe was used to measure $i_{L\rm w}$, and GW Instek GTP-200B-4 voltage probes were used to measure $v_{C\rm u}$, and $v_{\rm dc}$. Imperix B-Box RCP 3.0 was used for control and PWM generation.

Experimental results

The operating conditions of the experiments performed on the Y-inverter prototype are summarized in Table III along with the corresponding measured efficiency values. Fig.5, Fig.6, Fig.7, and Fig.8 show the experimental waveforms when the Y-inverter operated in the buck-only mode, whereas Fig.9, Fig.10, Fig.11, and Fig.12 show the experimental waveforms when the Y-inverter operated in the buck-boost mode. Fig. 13 shows the measured efficiency values for different load RMS voltages where the data points in Fig. 13 (a) and Fig. 13 (b) are grouped based on the output power values, which are relatively close to each other in each group.

The boundary between the buck-only and the buck-boost modes corresponds to operating conditions where $v_{\rm dc} = \hat{v_C}$. These operating conditions are depicted in the Table III, and correspond to the data where the load RMS voltage is 49.5 V ($v_{\rm dc} = \hat{v_C} = 140\,\text{V}$). The data in Table III and Fig. 13 shows that the SPWM results in higher efficiency when the Y-inverter operates in the buck-only operation, while DPWM results in higher efficiency when the Y-inverter operates in the buck-boost operation.

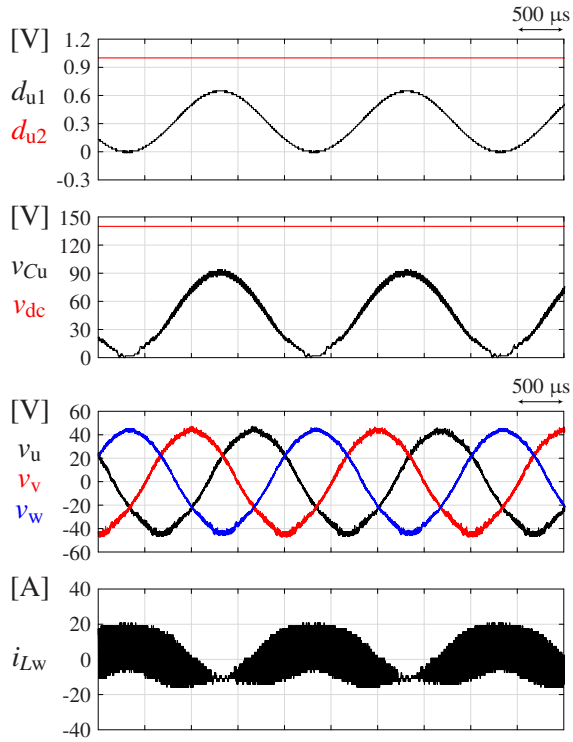

Fig. 5: Experimental waveforms when $\hat{v_C} = 90\,\mathrm{V}$, $f_o = 500\,\mathrm{Hz}$, $P_o = 599\,\mathrm{W}$, and SPWM is used.

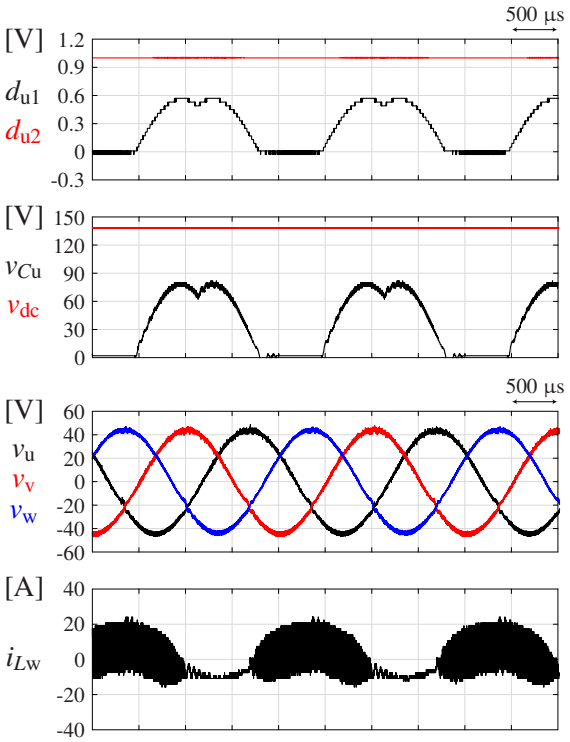

Fig. 6: Experimental waveforms when $\hat{v_C} = 90\,\mathrm{V}$, $f_o = 500\,\mathrm{Hz}$, $P_o = 599\,\mathrm{W}$, and DPWM is used.

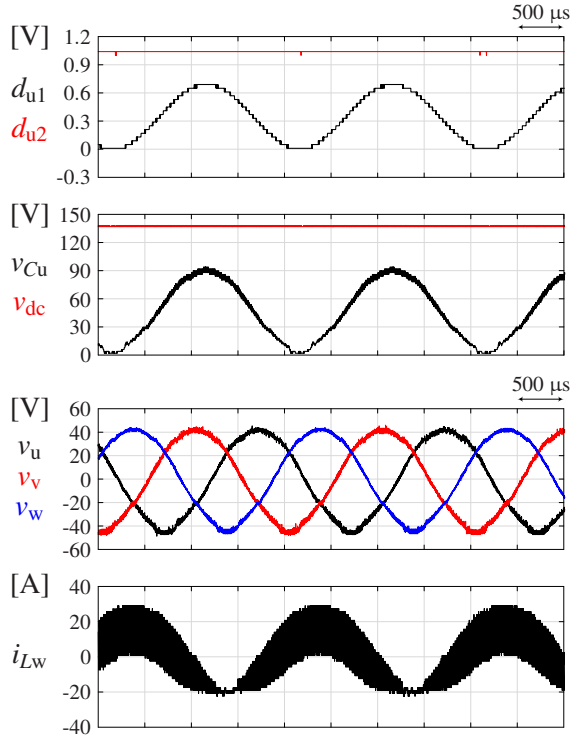

Fig. 7: Experimental waveforms when $\hat{v_C} = 90\,\mathrm{V}$, $f_o = 500\,\mathrm{Hz}$, $P_o = 1184\,\mathrm{W}$, and SPWM is used.

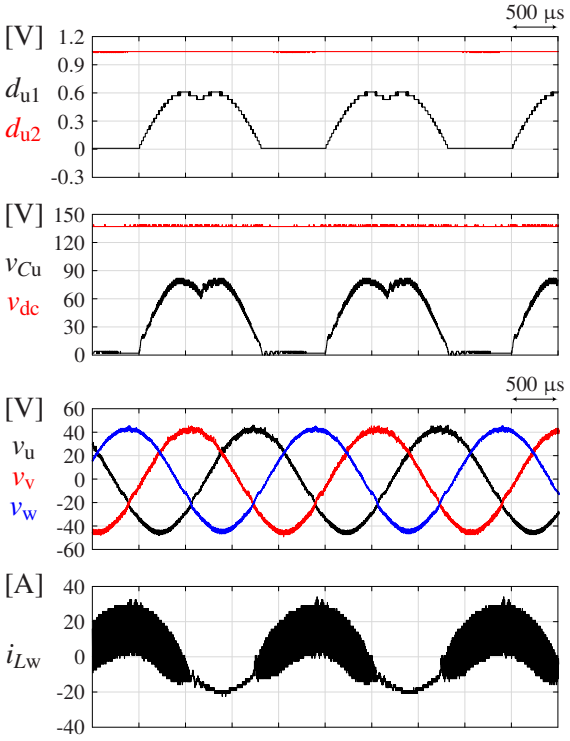

Fig. 8: Experimental waveforms when $\hat{v_C} = 90\,\mathrm{V}$, $f_o = 500\,\mathrm{Hz}$, $P_o = 1184\,\mathrm{W}$, and DPWM is used.

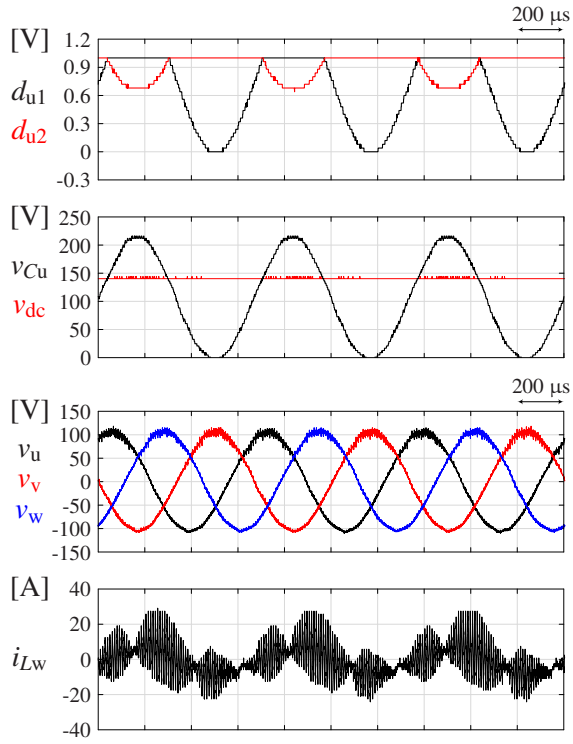

Fig. 9: Experimental waveforms when $\hat{v_C} = 210\,\mathrm{V}$, $f_o = 1.5\,\mathrm{kHz}$, $P_o = 601\,\mathrm{W}$, and SPWM is used.

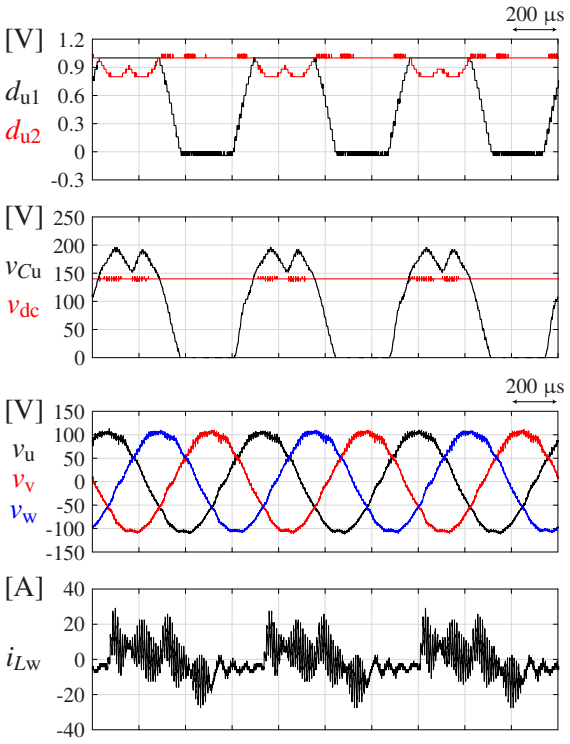

Fig. 10: Experimental waveforms when $\hat{v_C} = 210\,\mathrm{V}$, $f_o = 1.5\,\mathrm{kHz}$, $P_o = 601\,\mathrm{W}$, and DPWM is used.

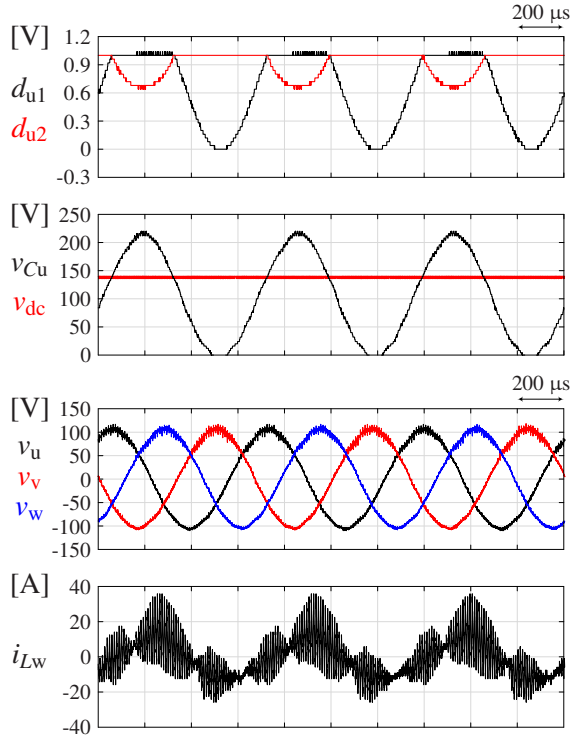

Fig. 11: Experimental waveforms when $\hat{v_C} = 210\,\mathrm{V}$, $f_o = 1.5\,\mathrm{kHz}$, $P_o = 1316\,\mathrm{W}$, and SPWM is used.

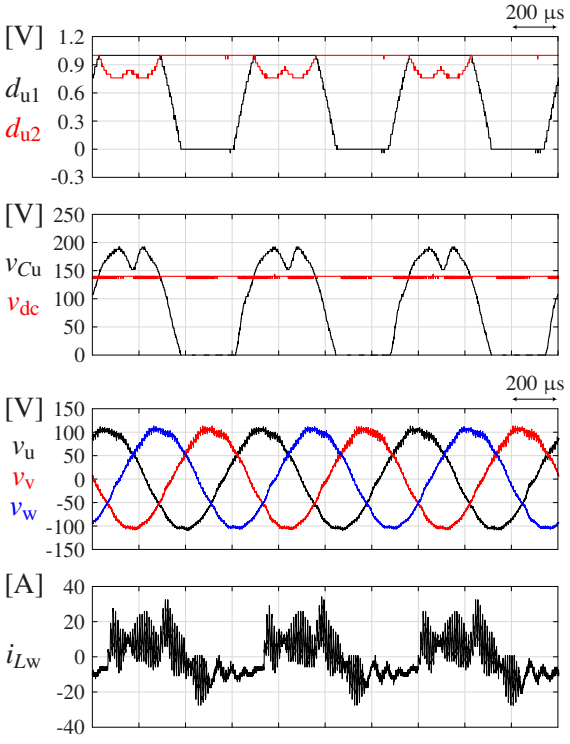

Fig. 12: Experimental waveforms when $\hat{v_C} = 210\,\mathrm{V}$, $f_o = 1.5\,\mathrm{kHz}$, $P_o = 1316\,\mathrm{W}$, and DPWM is used.

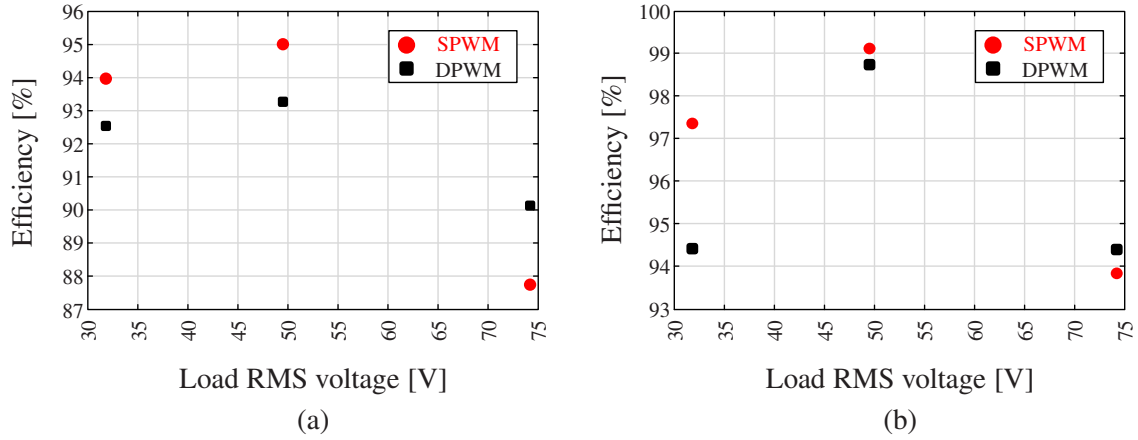

Fig. 13: Visualization of Table III data where (a) corresponds to lower power conditions, and (b) corresponds to higher power conditions.

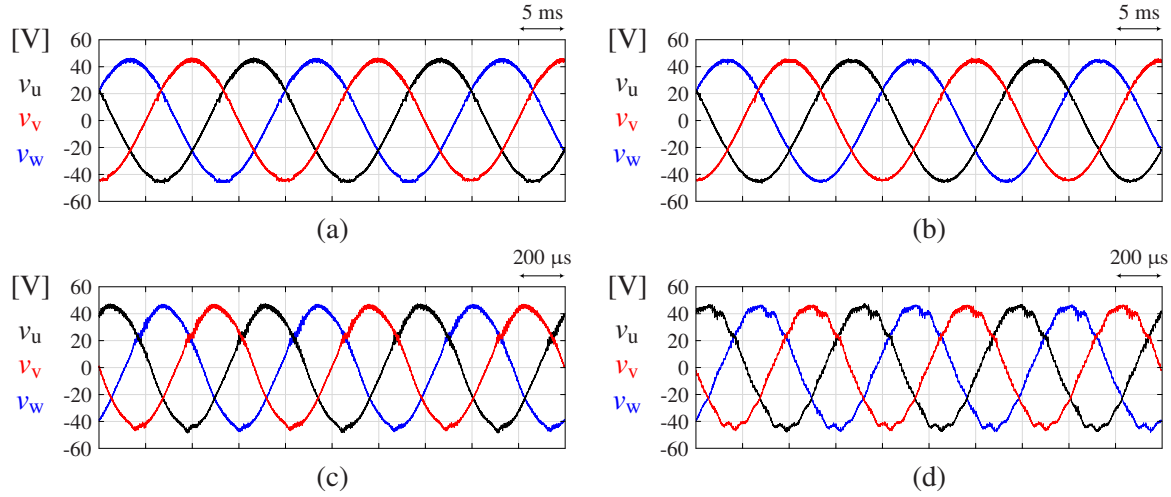

Fig. 14: Experimental phase-to-neutral voltages (a) when $f_o = 50\,\text{Hz}$, and SPWM is used, (b) when $f_o = 50\,\text{Hz}$, and DPWM is used, (c) when $f_o = 1.5\,\text{kHz}$, and SPWM is used, and (d) when $f_o = 1.5\,\text{kHz}$, and DPWM is used.

Although the DPWM reduces the switching losses, other losses appear to outweigh the reduction of the switching losses during the buck-only operation. These results show that there is a potential for the development of a hybrid PWM scheme in which SPWM is used during the buck-only operation and DPWM is used during the buck-boost operation. A detailed theoretical analysis of the losses should be done and it is left for future work.

Besides the effect of the modulation scheme on efficiency, the effect on the voltage quality has been investigated. Carefully looking at v_{Cu} in Fig. 10 and Fig. 12, a distortion in f_o voltage component can be observed. To further investigate the effect of f_o and the modulation scheme on the load voltage quality, the phase-to-neutral voltages were measured for relatively low and relatively high values of f_o and for both DPWM and SPWM.

Fig. 14 shows the phase-to-neutral voltages, where the corresponding circuit parameters are shown in Table II. In Fig. 14 (a) and Fig. 14 (c) SPWM is used, while in Fig. 14 (b) and Fig. 14 (d) DPWM is used. In Fig. 14 (a) and Fig. 14 (b), $f_o = 50\,\text{Hz}$, while in Fig. 14 (c) and Fig. 14 (d), $f_o = 1.5\,\text{kHz}$. As shown in Fig. 14, as the f_o increases, more pronounced distortion of the output waveforms is detected. Clearly, the value of f_o where distortion becomes non-negligible depends on both the switching frequency and the values of L and C used in the design of the power cell. These findings have been confirmed by simulations

as well, although not shown in this paper. Taking the aforementioned findings into consideration, it is possible to conclude that the switching frequency cannot simply be increased further, and that an appropriate selection of the L and C values should be considered

Conclusion

This paper has highlighted differences in the use of SPWM and DPWM schemes at the boundary of the operational regimes of the Y-Inverter in motor-drive applications. The results indicate that inverter performance optimization should include the possibility of hybrid modulation schemes (i.e., applying DPWM when the motor operates at low-torque high-speed conditions and SPWM at low-speed high-torque conditions). The development of an algorithm that enables automatic selection of the modulation strategy depending on the instantaneous operational condition is under study.

References

[1] R. Amorim Torres, H. Dai, W. Lee, B. Sarlioglu and T. Jahns, "Current-Source Inverter Integrated Motor Drives Using Dual-Gate Four-Quadrant Wide-Bandgap Power Switches," in IEEE Transactions on Industry Applications, vol. 57, no. 5, pp. 5183-5198, Sept.-Oct. 2021, doi: 10.1109/TIA.2021.3096179.

[2] R. A. Torres, H. Dai, W. Lee, T. M. Jahns and B. Sarlioglu, "Current-Source Inverters for Integrated Motor Drives using Wide-Bandgap Power Switches," 2018 IEEE Transportation Electrification Conference and Expo (ITEC), 2018, pp. 1002-1008, doi: 10.1109/ITEC.2018.8450127.

[3] M. Antivachis, D. Bortis, L. Schrittwieser and J. W. Kolar, "Three-phase buck-boost Y-inverter with wide DC input voltage range," 2018 IEEE Applied Power Electronics Conference and Exposition (APEC), 2018, pp. 1492-1499, doi: 10.1109/APEC.2018.8341214.

[4] M. Antivachis, N. Kleynhans and J. W. Kolar, "Three-Phase Sinusoidal Output Buck-Boost GaN Y-Inverter for Advanced Variable Speed AC Drives," in IEEE Journal of Emerging and Selected Topics in Power Electronics, vol. 10, no. 3, pp. 3459-3476, June 2022, doi: 10.1109/JESTPE.2020.3026742.